

Learning Interpretable, High-Performing Policies for Continuous Control Problems

Rohan Paleja*, Yaru Niu*, Andrew Silva, Chace Ritchie, Sugju Choi, Matthew Gombolay
 Atlanta, GA 30332
 Georgia Institute of Technology
 {rohan.paleja, yaruniu, andrew.silva, critchie7, schoi424, matthew.gombolay}@gatech.edu

Abstract

Gradient-based approaches in reinforcement learning (RL) have achieved tremendous success in learning policies for continuous control problems. While the performance of these approaches warrants real-world adoption in domains, such as in autonomous driving and robotics, these policies lack interpretability, limiting deployability in safety-critical and legally-regulated domains. Such domains require interpretable and verifiable control policies that maintain high performance. We propose Interpretable Continuous Control Trees (ICCTs), a tree-based model that can be optimized via modern, gradient-based, RL approaches to produce high-performing, interpretable policies. The key to our approach is a procedure for allowing direct optimization in a sparse decision-tree-like representation. We validate ICCTs against baselines across six domains, showing that ICCTs are capable of learning interpretable policy representations that parity or outperform baselines by up to 33% in autonomous driving scenarios while achieving a 300x-600x reduction in the number of policy parameters against deep learning baselines.

1 Introduction

Reinforcement learning with deep function approximators has enabled the generation of high-performance continuous control policies across a variety of complex domains, from robotics [35] and autonomous driving [54] to protein folding [26] and traffic regulation

[15]. While the performance of these policies opens up the possibility of real-world adoption in domains such as autonomous driving and robotics, the conventional deep-RL policies used in prior work [35, 54, 15] lack interpretability, limiting deployability in safety-critical and legally-regulated domains [17, 33, 10, 52]. White-box approaches, as opposed to typical black-box deep neural networks used in deep-RL, model decision processes in a human-readable representation. Such approaches afford interpretability, allowing end-users to gain insight into the model’s decision-making behavior. Utilizing white-box approaches within machine learning can help to build trust, ensure safety, and enable end-users to inspect policies before deploying them to the real world [39, 25, 3]. In this work, we present a novel tree-based architecture that afford gradient-based optimization with modern RL techniques to produce high-performance, interpretable policies for continuous control problems. Continuous control problems present a difficult challenge, encompassing real-world problems from high-speed autonomous driving [54] to autopilots for landing spacecraft [4].

Prior work has attempted to approximate interpretability in deep networks through explanations of each layer [39, 28] or by explanations generated through separate networks [25, 3]. While these approaches can help to partially explain the behavior of a control policy, the explanations are not guaranteed to be accurate or generally applicable across the state-space, leading to erroneous conclusions and a lack of accountability of predictive models [44]. In contrast to local explanations, an *interpretable model* provides a transparent *global* representation of a policy’s behavior. This model can be understood directly by its structure and parameters (e.g., linear models, decision trees, and our ICCTs) [14], offering verifiability and guarantees that are not afforded by post-hoc explainability frameworks. Few works have attempted to learn an interpretable model directly; rather, prior work has attempted policy distillation to a decision

* Authors contributed equally to this work.

[18, 7, 55] or imitation learning via a decision tree across trajectories generated via a deep model [8], leaving much to be desired. Interpretable reinforcement learning remains an open challenge [45].

In this work, we directly produce high-performance, interpretable continuous control policies represented by a minimalistic tree-based architecture augmented with low-fidelity linear controllers. We provide the following contributions:

1. We propose Interpretable Continuous Control Trees (ICCTs), a novel tree-based model that can be optimized via gradient descent with modern RL algorithms to produce high-performance, interpretable continuous control policies. We provide several extensions to prior DDT frameworks to increase expressivity (Section 4.2.3) and allow for direct optimization on a sparse decision-tree-like representation (Section 4.2.1-4.2.2).
2. We show that our ICCTs are universal function approximators and can thus be utilized to learn continuous control policies in any domain (Section 5) assuming that the ICCT has a reasonable depth (complexity).
3. We empirically validate ICCTs across six continuous control domains, including three from the autonomous driving simulator, Flow [54] (Section 7). To the best of our knowledge, we are the first work to develop a high-performing, interpretable tree-based framework for continuous control.

2 Related Work

Explainable AI (xAI) is concerned with understanding and interpreting the behavior of AI systems [36]. In recent years, the necessity for human-understandable models has increased greatly for safety-critical and legally-regulated domains, many of which involve continuous control [29, 17]. Continuous control problems are apparent throughout robotics [27, 23], encountered in any domain where actions cannot be broken down into discrete units (e.g., specifying joint torques for a robot arm or the steering angle for an autonomous vehicle). In such domains, prior work [46, 35, 19, 22] has typically used highly-parameterized deep neural networks in order to learn high-performance policies, completely lacking in model transparency.

Interpretable machine learning approaches refers to a subset of xAI techniques that produce globally transparent policies (i.e., humans can inspect the entire model, as in a decision tree [11, 6, 40] or rule list [2, 53, 33, 13]). Tree-based Frameworks are of particular importance to our work. Decision trees [11]

represent a hierarchical structure where an input decision can be traced to an output via evaluation of decision nodes (i.e., “test” on an attribute) until arrival at a leaf node. Decision nodes within the tree are able to split the problem space into meaningful subspaces, simplifying the problem as the tree gets deeper [32, 30, 50]. Decision trees also provide *global* explanations of a decision-making policy that are valid throughout the input space [5], as opposed to local explanations typically provided via “post-hoc” explainability techniques [43]. Explainability stands in contrast to interpretability, as explanations may fail to capture the true decision-making process of a model or may apply only to a local region of the decision-space, thereby preventing a human from building a clear or accurate mental model of the entire policy [44, 37, 1].

Recently, [45] presented a set of grand challenges in interpretable machine learning to guide the field towards solving critical research problems that must be solved before machine learning can be safely deployed within the real world. In this work, we present a solution to directly assess two challenges: (1) Optimizing sparse logical models such as decision trees and (10) Interpretable reinforcement learning. We propose a novel high-performing, interpretable, and sparse architecture, Interpretable Continuous Control Trees (ICCTs), directly allowing end-users to inspect and understand the decision-making policy.

3 Preliminaries

In this section, we present background information on differentiable decision trees (DDTs), a “crispification” procedure prior work has utilized to translate DDTs into decision trees and its drawbacks, and reinforcement learning.

3.1 Differentiable Decision Trees (DDTs)

Prior work has proposed differentiable decision trees (DDTs) [49, 48] – a neural network architecture that takes the topology of a decision tree (DT). Similar to a decision tree, DDTs contain decision nodes and leaf nodes; however, each decision node within the DDT utilizes a sigmoid activation function (“soft” decision) instead of a Boolean decision (“hard” decision). Each decision node, i , represented by a sigmoid activation function, displayed in Equation 1.

$$y_i = \frac{1}{1 + \exp(-\alpha(\vec{w}_i \cdot \vec{x} - b_i))} \quad (1)$$

Here, the features vectors describing the current state, \vec{x} , are weighted by \vec{w}_i , and a splitting criterion, b_i , is subtracted to form the splitting rule. y_i is the probability of decision node i evaluating to TRUE and α

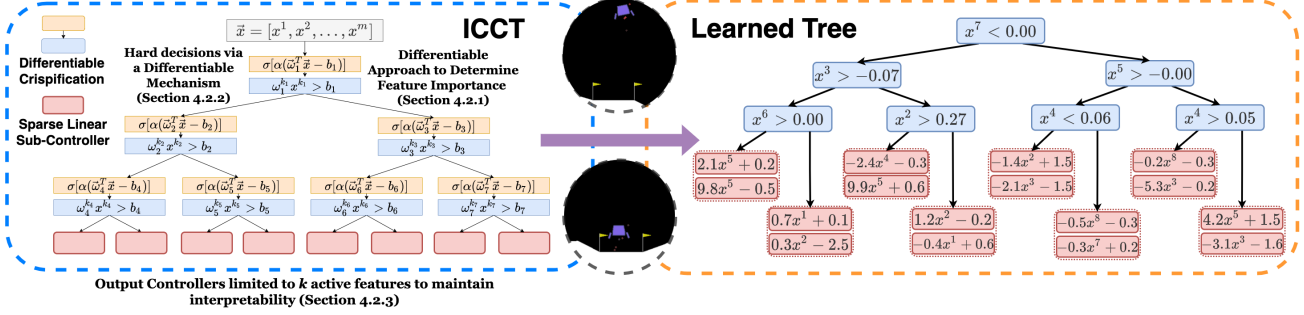


Figure 1: The ICCT framework (left) displays decision nodes and sparse linear leaf controllers with pointers to sections discussing our contributions (assuming $\alpha > 0$). A learned representation of a high-performing ICCT policy in Lunar Lander (right) displays the interpretability of our ICCTs. Each decision node is conditioned upon only a single feature and the sparse linear controllers (to control the main engine throttle and left/right thrusters) are set to have only **one** active feature. The action dimension is 2 in this example.

governs the steepness of the sigmoid activation, where $\alpha \rightarrow \infty$ results in a step function. Prior work with discrete-action DDTs modeled each leaf node with a probability distribution over possible output classes [48, 41]. Leaf node distributions are then summed weighted by the likelihood of reaching the leaf to produce a final action distribution over possible outputs.

3.1.1 Conversion of a DDT to a DT

DDTs with decision nodes represented in the form of Equation 1 are not interpretable. As DDTs maintain a one-to-one correspondance to DTs with respect to their structure, prior work [48, 41] proposed methodology to convert a DDT into an interpretable decision tree (a process termed “crispification”). In this subsection, we discuss the crispification methodology used in prior work and its drawbacks.

To create an interpretable, “crisp” tree from a differentiable form of the tree, prior work adopted a simplistic procedure. Starting with the differentiable form, prior work first converts each decision node from a linear combination of all variables into a single feature check (i.e., a 2-arity predicate with a variable and a threshold). The feature reduction is accomplished by considering the feature corresponding to the weight with the largest magnitude, $k = \arg \max_j |w_j^i|$, resulting in the decision node representation $y_i = \sigma(\alpha(w_i^k x^k - b_i))$. The sigmoid steepness, α , is also set to infinity, resulting in a “hard” decision (branch left OR right) [48, 41]. After applying this procedure to each decision node, decision nodes are represented by $y_i = (w_i^k x^k - b_i > 0)$

As each leaf node is represented as a probability mass function over output class in prior work, leaf nodes, l , must be modified to produce a single output class, o during crispification. As such, we can apply an argument max, $o_d = \arg \max_a |l_d^a|$, to find the maximum

valued class within the d^{th} leaf distribution.

Drawbacks: This simplistic crispification procedure results in a crisp tree that is inconsistent with the original DDT (model differences arise from each argmax operation) and thus, is not applicable to complex continuous control domains as we show in Section 7.

In our work, we design a novel architecture that is able to update its parameters via gradient descent while maintaining an interpretable decision-tree-like representation, thereby avoiding any inconsistencies generated through a crispification procedure. To the best of our knowledge, we are the first work to deploy an interpretable tree-based framework for continuous control.

3.2 Reinforcement Learning (RL)

A Markov Decision Process (MDP) M is defined as a 6-tuple $\langle S, A, R, T, \gamma, \rho_0 \rangle$. S is the state-space, A is the action-space, $R(s, a)$ is the reward received by an agent for executing action, a , in state, s , $T(s'|s, a)$ is the probability of transitioning from state, s , to state, s' , when applying action, a , $\gamma \in [0, 1]$ is the discount factor, and $\rho_0(s)$ is the initial state distribution. A policy, $\pi(a|s)$, gives the probability of an agent taking action, a , in state, s . The goal of RL is to find the optimal policy, $\pi^* = \arg \max_{\pi} \mathbb{E}_{\tau \sim \pi} \left[\sum_{t=0}^T \gamma^t R(s_t, a_t) \right]$ to maximize cumulative discounted reward, where $\tau = \langle s_0, a_0, \dots, s_T, a_T \rangle$ is an agent’s trajectory. In this work, while ICCTs are framework-agnostic (i.e., ICCTs will work with any update rule), we proceed with Soft Actor-Critic (SAC) [22] as our RL algorithm. The actor objective within SAC is given in Equation 2, where $Q_w(s_t, a_t)$ is expected, future discounted reward as learned by a given function approximator.

$$J_{\pi}(\theta) = \mathbb{E}_{s_t \sim \mathcal{D}} [\mathbb{E}_{a_t \sim \pi_{\theta}} [\alpha \log(\pi_{\theta}(a_t|s_t)) - Q_w(s_t, a_t)]] \quad (2)$$

4 Method

In this section, we introduce our Interpretable Continuous Control Trees (ICCTs), a novel extension to prior DDT-based frameworks. Our ICCTs are able to maintain interpretability while representing high-performance continuous control policies via a differentiable crispification procedure allowing for optimization in a sparse decision-tree like representation, and the addition of sparse linear leaf controllers to increase expressivity while maintaining legibility.

4.1 ICCT Architecture

Our ICCTs are initialized to be a symmetric decision tree with l decision leaves and $l-1$ decision nodes (tree depth by $\log_2(l)$). Each decision leaf is represented by a linear sparse controller that is parameterized by \vec{x} . Decisions are routed via decision nodes towards a leaf controller, which is then used to produce the continuous control output. Our ICCT is similar to hierarchical models which maintain a high-level controller over several low-level controllers. Prior work has shown this to be a successful paradigm in continuous control [38].

Each decision node, i , has an activation steepness weight, α , associated weights, \vec{w}_i , with cardinality, m , matching that of the input feature vector, \vec{x} , and a scalar bias term, b_i . Each leaf node, l_d , where $d \in \{1, \dots, l\}$, contains per-leaf weights, $\vec{\beta}_d \in \mathbb{R}^{|m|}$, per-leaf selector weights that learn the relative importance of candidate splitting criterion, $\vec{\theta}_d \in \mathbb{R}^{|m|}$, per-leaf bias terms, $\vec{\phi}_d \in \mathbb{R}^{|m|}$, and per-leaf scalar standard deviations, γ_d . We note that, if the continuous action space is multi-dimensional, then *only* the leaf controllers (and associated weights) are expanded across $|A|$ dimensions, where $|A|$ is the cardinality of the action space. For each action, the mean of the output action distribution is represented by the linear controller, $\vec{\beta}_d^T \vec{x} - \vec{\phi}_d$, for leaf d , where the output action can be determined via sampling ($a \sim \mathcal{N}(\vec{\beta}_d^T \vec{x} - \phi_d, \gamma_d)$) during training and directly via the mean during runtime. We display an example tree in Figure 1. After the differentiable crispification procedure, which we further discuss in Sections 4.2.1 and 4.2.2, our model representation follows that of a decision tree with linear controllers at the leaves.

While decision trees (DT) are generally considered interpretable [33], trees of arbitrarily large depths can be difficult to understand [20] and simulate [37]. A sufficiently sparse DT is desirable and considered interpretable [31]. Utilizing linear controllers at the leaves also allows us to maintain interpretability, as linear controllers are widely used and generally considered interpretable for humans [24]. However, simi-

larly, for large feature spaces typically encountered in real-world problems, such a controller would not be interpretable. In our work, we augment *sparse* linear controllers at the leaves to balance the trade-off between sparsity/complexity in logic (static vs. sub-controller leaves) and model depth, and performance. We discuss the procedure for doing so in Section 4.2.3.

4.2 ICCT Key Elements

In this section, we discuss our ICCT’s procedure for determining an action given an input feature via a decision-process that is completely interpretable. Note that during both training via reinforcement learning and deployment, our ICCT configuration is interpretable and thus, our inference of an action must allow gradient flow. We present a novel approach that allows for direct optimization of sparse logical models via an online differentiable crispification procedure to determine feature importance (Section 4.2.1) and allow for hard decisions (Section 4.2.2). In Algorithm 1, we provide general pseudocode representing our ICCT’s decision-making process.

Algorithm 1 ICCT Action Determination

Input: ICCT $I(\cdot)$, state feature $\vec{x} \in S$, controller sparsity e , training flag $t \in \{True, False\}$

Output: $a \in \mathbb{R}^{|a|}$

- 1: $\sigma(\alpha(w_i^k x^k - b_i)) \leftarrow \text{NODE_CRISP}(\sigma(\alpha(\vec{w}_i^T \vec{x} - b_i)))$
 - 2: $\alpha(w_i^k x^k - b_i) > 0 \leftarrow \text{OUTCOME_CRISP}(\sigma(\alpha(w_i^k x^k - b_i)))$
 - 3: $l_d \leftarrow \text{INTERPRETABLE_NODE_ROUTING}(\vec{x})$
 - 4: $l_d^* \leftarrow \text{ENFORCE_CONTROLLER_SPARSITY}(e, l_d)$
 - 5: **if** t **then**
 - 6: $a \sim \mathcal{N}(l_d^*(\vec{x}), \gamma_d)$
 - 7: **else**
 - 8: $a \leftarrow l_d^*(\vec{x})$
 - 9: **end if**
-

At each timestep, the ICCT model, $I(\cdot)$, receives a state feature, \vec{x} . To determine an action in an interpretable form, in Steps 1 and 2 of Algorithm 1, we start by applying the differentiable crispification approaches of `NODE_CRISP` and `OUTCOME_CRISP` to decision nodes so that each decision node is only conditioned upon a single variable (Section 4.2.1, and the evaluation of a decision node results in a Boolean (Section 4.2.2), respectively. Once the operations are completed, in Step 3, we can utilize \vec{x} and logically evaluate each decision node until arrival at a linear leaf controller (`INTERPRETABLE_NODE_ROUTING`). The linear leaf controller is then modified, in Step 4, to only condition upon e features, where e is a sparsity parameter specified a priori (Section 4.2.3). Finally, an action can be determined via sampling from a Gaussian distribution conditioned upon the mean generated via the input-parameterized sparse leaf controller, l_d^* , and

scalar variance maintained within the leaf, γ_d , (Step 6) during training or directly through the outputted mean (Step 8) during runtime.

4.2.1 Decision Nodes Crispification

The `NODE_CRISP` procedure in Algorithm 1 conditions each decision node to split upon a single dimension of \vec{x} . Instead of using a non-differentiable argmax function [48], we utilize a softmax function, also known as softargmax [21], described by Equation 3. In this equation, we denote the softmax function as $f(\cdot)$, which takes as input a set of class weights and produces class probabilities. \vec{w}_i represents a categorical distribution with class weights, individually denoted by w_i^j , and τ is the temperature, determining the steepness of $f(\cdot)$.

$$f(\vec{w}_i)_k = \frac{\exp\left(\frac{w_i^k}{\tau}\right)}{\sum_j^m \exp\left(\frac{w_i^j}{\tau}\right)} \quad (3)$$

While setting the temperature near-zero would satisfy our objective of producing a one-hot vector, where the outputted class probability of the index of the most impactful feature would be one, this operation can lead to vanishing gradients. We therefore set τ equal to 1, and utilize a `one_hot` function, where the `one_hot` produces a one-hot vector with the element associated with the highest-weighted class set to one and all other elements set to zero. We display an equation for our differentiable procedure for determining the largest magnitude weight in Equation 4, where $g(\cdot)$ is the `one_hot` function.

$$\vec{z}_i = g(f(|\vec{w}_i|)) \quad (4)$$

The one-hot encoding \vec{z}_i can be multiplied by the original weights to produce a new set of weights with only one active weight, $\vec{z}_i^T \vec{x} \rightarrow w_i^k$. Accordingly, the decision node representation is transferred from $\sigma(\alpha(\vec{w}_i^T \vec{x} - b_i)) \rightarrow \sigma(\alpha(w_i^k x^k - b_i))$, where k is the index of the most impactful feature.. We maintain differentiability in the procedure described in Equation 4 by utilizing the straight-through trick [9]. Below, we conduct a short example detailing our procedure.

Example: Say we have a two-leaf decision tree (one decision node) with an input feature, $\vec{x} = [2, 3]$ with a cardinality of 2 (i.e. $m = 2$), associated weights of $\vec{w}_1 = [2, 1]^T$, and a bias term b_1 of 1. The sigmoid steepness, α is also set equal to 1 for simplicity. It is easily seen that the most impactful weight within the decision node is $w_1^1 = 2$. Utilizing Equation 4, we can compute $\vec{z}_1 = [1, 0]$. Multiplying \vec{z}_1 to the original weights, \vec{w}_1 and input feature, \vec{x} , and scaling by α , we have an crisp decision node $\sigma(2x^1 - 1)$ or $\sigma(3) = 0.95$.

4.2.2 Decision Outcome Crispification

Here, we describe the second piece of our online differentiable crispification procedure, `OUTCOME_CRISP` in Algorithm 1. `OUTCOME_CRISP` translates the outcome of a decision node so that the outcome is a Boolean decision rather than a set of probabilities generated via a sigmoid function (i.e., $p = y_i$ for True/Left Branch and $q = 1 - y_i$ for False/Right Branch). First, we create a vector representation of the decision node output $\vec{v}_i = [\alpha(w_i^k x^k - b_i), 0]$, for the i^{th} decision node. Placing \vec{v}_i through a softmax operation, we can produce the probability of tracing down the left branch or right. We can then apply a one-hot operation to produce a hard decision of whether to branch left or right, denoted by y_i and described by Equation 5. Essentially, the decision node will evaluate to True if $\alpha(w_i^k x^k - b_i) > 0$ and right otherwise.

$$y_i = g(f(\vec{v}_i)) \quad (5)$$

We note this procedure is highly similar to that in Equation 4 with the former input being $|\vec{w}_k|$ and the latter input being \vec{j}_i . We generalize this procedure to a function call within the supplementary material, including operations to maintain the gradient via the straight-through trick.

Example: Continuing the example in Section 4.2.1, we can take the outputted crisp decision node and generate a vector $\vec{v}_i = [2x^1 - 1, 0]$, or by substituting the input feature, $\vec{v}_i = [3, 0]$. Performing the operations specified in Equation 5, we receive the intermediate output from the softmax $[.95, .05]$ (rounded to two decimal places) and $y_1 = [1, 0]$ after performing the `one_hot` operation, denoting that the decision-tree should follow the left branch.

Conversion to a Simple Form: The above crispification process produces decision-tracing equal to that of a DT. The node representation can be further simplified to represent that of Figure 1. Each crisp decision node, i , can be reduced algebraically to $x^k > \frac{b_i}{w_i^k}$ (given $w_i^k > 0$).

4.2.3 Sparse Linear Leaf Controllers

This section describes the procedure to translate a linear leaf controller to condition upon e features (`ENFORCE_CONTROLLER_SPARSITY` procedure in Algorithm 1), enforcing sparsity within the sub-controller and thereby, enhancing ICCT interpretability. As noted in Section 4.1, our ability to utilize sparse sub-controllers allows us to balance the interpretability-performance tradeoff. The sparsity of the linear sub-controllers ranges from setting $e = 0$ and maintaining static leaf distributions (denoted ICCT-static in Section 7) to $e = m$ (denoted ICCT-complete

in Section 7). Empirically, one can optimize for both interpretability and performance by starting with ICCT-complete and reduce e such that e is as small as possible while preserving performance. In Section 7, we see that in many cases, ICCT-static ($e = 0$) can perform competitively and even outperform a MLP.

Equation 6 displays the procedure for determining a `k_hot` encoding, \vec{u}_d , that represents the k most impactful selection weights within a leaf’s linear controller. The `k_hot` function, denoted by $h(\cdot)$, takes as input a vector of class weights and returns an equal-dimensional vector with k elements set to one. The indexes associated with the elements set to one match that of the k highest-weighted elements within the input feature.

$$\vec{u}_d = h(f(|\vec{\theta}_d|)) \quad (6)$$

We maintain differentiability through the operation in Equation 5 by utilizing the straight-through trick [9]. In Equation 7, we can transform a complete (all weights active) sub-controller, for leaf d , into a sparse sub-controller.

$$I_d^* = (\vec{u}_d \circ \vec{\beta}_d)^T (\vec{u}_d \circ \vec{x}) + \vec{u}_d^T \vec{\phi}_d \quad (7)$$

A depiction of the sparse sub-models can be seen at the bottom of Figure 1, where the sparsity of the sub-controllers, e , is set to 1 and the dimension of the action space is 2.

5 Universal Function Approximation

In this section, we provide a proof to show our ICCTs are universal function approximators, that is, can represent any decision surface given enough parameters. Our ICCT architecture consists of successive indicator functions, whose decision point lies among a single dimension of the feature space, followed by a linear controller to determine a continuous control output. For simplicity, we assume below that the leaf nodes contain static distributions. However, maintaining a linear controller at the leaves is more expressive and thus, the result below generalizes directly to ICCTs.

The decision-making of our ICCTs can be decomposed as a sum of products. In Equation 8, we display a computed output for a 4-leaf tree, where decision node outputs, y_i , are determined via Equation 1. Here, the sigmoid steepness, α is set to infinity (transforming the sigmoid function into an indicator function) resulting in hard decision points ($y_i \in \{0, 1\}$). Equation 8 shows that the chosen action is determined by computation of probability of reaching a leaf, y , multiplied by static tree weights maintained at the distribution, p .

$$\begin{aligned} ICCT(x) = & p_1(y_1 * y_2) + p_2(y_1 * (1 - y_2)) \\ & + p_3((1 - y_1) * y_3) + p_4 * ((1 - y_1) * (1 - y_3)) \end{aligned} \quad (8)$$

Equation 8 can be directly simplified into the form of $G(x) = \sum_{j=1}^N p_j \sigma(w_j^T x + b_j)$, similar to Equation 1 in [16]. [16] demonstrates that finite combination of fixed, univariate functions can approximate any continuous function. The key difference between our architecture is that our univariate function is an indicator function rather than the commonly used sigmoid function. Below, we provide two lemmas to show that indicator functions fall within the space of univariate functions specified by [16].

Lemma 1 *An indicator function is sigmoidal.*

Proof: This follows from the definition of sigmoidal: $\sigma(t) \rightarrow 1$ as $t \rightarrow \infty$ and $\sigma(t) \rightarrow 0$ as $t \rightarrow -\infty$.

Lemma 2 *An indicator function is discriminatory.*

Proof: As an indicator function is bounded and measurable, by Lemma 1 of [16], it is discriminatory.

Theorem 1 *Let σ be any continuous discriminatory function. ICCTs are universal function approximators, that is, dense in the space of $C(I_n)$. In other words, there is a representation of ICCTs, $I(x)$, for which $|I(x) - f(x)| < \epsilon$ for all $x \in I_n$, for any function, f ($f \in C(I_n)$), where $C(I_n)$ denotes the codomain of an n -dimensional unit cube, I_n .*

Proof: As the propositional conditions hold for Theorem 1 in [16], the result that ICCTs are dense in $C(I_n)$ directly follows. We note that as the indicator function jump-continuous, we refer readers to [47] whom extend UFA for $G(x) = \sum_{j=1}^N p_j \sigma(w_j^T x + b_j)$ to the case when σ is jump-continuous.

6 Environments

We provide short descriptions of each continuous control domain used in our extensive evaluation.

Inverted Pendulum: In Inverted Pendulum [51], a control policy must apply throttle to balance a pole.

Lunar Lander: In Lunar Lander [42, 12], a policy must throttle main engine and side engine thrusters for a lander to land on a specified landing pad.

Lane-Keeping [34]: A control policy must control a vehicle’s steering angle to stay within a curving lane.

Flow Single-Lane Ring Network [54]: A control policy must apply acceleration commands to a vehicle agent to stabilize traffic flow consisting of 21 other human-driven (synthetic) vehicles.

Flow Multi-Lane Ring Network [54]: A policy must apply acceleration and lane-changing commands

Table 1: In this table, we display the results of our evaluation. For each evaluation, we report the mean (\pm standard error) and the complexity of the model required to generate such a result. Our table is broken into three segments, the first containing equally interpretable approaches that utilize static distributions at their leaves. The second segment contains interpretable approaches that maintain linear controllers at their leaves. The ordering of methods denotes the relative interpretability. The third segments displays black-box approaches. We bold the highest-performing method in each segment, and break ties in performance by model complexity.

Method	Common Continuous Control Problems			Flow Autonomous Driving Problems		
	Inverted Pendulum	Lunar Lander	Lane Keeping	Single-Lane Ring	Multi-Lane Ring	Figure-8
DT	155.0 \pm 0.9 256 leaves (766 params)	-285.5 \pm 15.6 256 leaves (1022 params)	-359.0 \pm 11.0 256 leaves (766 params)	123.2 \pm 0.03 32 leaves (94 params)	503.2 \pm 24.8 256 leaves (1022 params)	831.1 \pm 1.1 256 leaves (766 params)
CDDT-Crisp ¹	5.0 \pm 0.0 2 leaves (7 params)	-451.6 \pm 97.3 8 leaves (53 params)	-43526.0 \pm 15905.0 16 leaves (77 params)	68.1 \pm 18.7 16 leaves (77 params)	664.5 \pm 192.6 16 leaves (109 params)	322.9 \pm 47.1 16 leaves (77 params)
ICCT-static	984.0 \pm 10.4 32 leaves (127 params)	192.4 \pm 10.7 32 leaves (221 params)	374.2 \pm 55.8 16 leaves (77 params)	120.5 \pm 0.5 16 leaves (77 params)	1271.7 \pm 4.1 16 leaves (109 params)	1003.8 \pm 27.2 16 leaves (77 params)
ICCT-1-feature	1000.0 \pm 0.0 8 leaves (45 params)	190.1 \pm 13.7 8 leaves (69 params)	437.6 \pm 7.0 16 leaves (77 params)	121.6 \pm 0.5 16 leaves (93 params)	1269.6 \pm 10.7 16 leaves (157 params)	1072.4 \pm 37.1 16 leaves (93 params)
ICCT-2-feature	1000.0 \pm 0.0 4 leaves (29 params)	258.4 \pm 7.0 8 leaves (101 params)	458.5 \pm 6.3 16 leaves (93 params)	121.9 \pm 0.5 16 leaves (125 params)	1280.4 \pm 7.3 16 leaves (237 params)	1088.6 \pm 21.6 16 leaves (125 params)
ICCT-3-feature	1000.0 \pm 0.0 2 leaves (17 params)	275.8 \pm 1.5 8 leaves (133 params)	448.8 \pm 3.0 16 leaves (109 params)	120.8 \pm 0.5 16 leaves (157 params)	1280.8 \pm 7.7 16 leaves (317 params)	1048.7 \pm 46.7 16 leaves (157 params)
ICCT-L1-sparse	1000.0 \pm 0.0 4 leaves (33 params)	265.2 \pm 4.3 8 leaves (181 params)	465.5 \pm 4.3 16 leaves (269 params)	121.5 \pm 0.3 16 leaves (781 params)	1275.3 \pm 6.7 16 leaves (2221 params)	993.2 \pm 14.6 16 leaves (525 params)
ICCT-complete	1000.0 \pm 0.0 2 leaves (15 params)	300.5 \pm 1.2 8 leaves (181 params)	476.6 \pm 3.1 16 leaves (269 params)	120.7 \pm 0.5 16 leaves (781 params)	1248.6 \pm 3.6 16 leaves (2221 params)	994.1 \pm 29.1 16 leaves (525 params)
CDDT-controllers Crisp ¹	84.0 \pm 10.4 2 leaves (15 params)	-126.6 \pm 53.5 8 leaves (181 params)	-39826.4 \pm 21230.0 16 leaves (269 params)	97.9 \pm 12.0 16 leaves (781 params)	639.62 \pm 160.4 16 leaves (2221 params)	245.5 \pm 48.5 16 leaves (525 params)
MLP-L	1000.0 \pm 0.0 86 params	231.6 \pm 49.8 124 params	474.7 \pm 5.8 134 params	121.8 \pm 0.6 155 params	646.4 \pm 151.2 229 params	868.4 \pm 100.9 107 params
MLP-U	1000.0 \pm 0.0 130 params	288.7 \pm 2.8 224 params	467.9 \pm 8.5 422 params	121.8 \pm 0.3 722 params	1239.5 \pm 4.2 3332 params	1077.7 \pm 31.1 1042 params
MLP-Max	1000.0 \pm 0.0 67589 params	298.5 \pm 0.7 69124 params	478.2 \pm 6.7 69634 params	121.7 \pm 0.4 77826 params	1011.9 \pm 141.3 83972 params	1104.3 \pm 9.4 73730 params
CDDT	1000.0 \pm 0.0 2 leaves (10 params)	226.4 \pm 44.5 8 leaves (102 params)	464.7 \pm 5.4 16 leaves (242 params)	120.9 \pm 0.5 16 leaves (708 params)	1248.0 \pm 6.4 16 leaves (1084 params)	1033.2 \pm 24.1 16 leaves (482 params)
CDDT-controllers	1000.0 \pm 0.0 2 leaves (18 params)	289.0 \pm 2.4 8 leaves (230 params)	469.7 \pm 11.1 16 leaves (434 params)	120.1 \pm 0.3 16 leaves (1412 params)	1243.8 \pm 3.6 16 leaves (3196 params)	1010.9 \pm 25.7 16 leaves (930 params)

to an ego vehicle to stabilize the flow of noisy traffic flow across multiple lanes.

Flow Figure-8 Network [54]: A control policy must apply acceleration to a vehicle to stabilize the flow in a Figure-8 network.

7 Results

In this section, we present the set of baselines we test our model against. Then we report the results of our approach versus these baselines across six continuous control domains, as shown in Table 1. All presented results are across five random seeds and all differentiable frameworks are trained via SAC [22]. Each tree-based framework is trained while maximizing performance and minimizing the complexity required to represent such a policy, thereby emphasizing interpretability. We release our anonymous codebase at <https://github.com/anonymous9628/ICCT>.

7.1 Baselines

We provide a list of baselines alongside abbreviations used for reference and brief definitions below.

¹As this model is derived via crispification [48], the complexity associated with this model is directly determined by its non-crisp counterpart.

- Continuous DDTs (CDDT): We translate the framework of [48] to function with continuous action-spaces by modifying the leaf nodes to represent static probability distributions. We refer readers to Section 3.1.1 for details of the procedure to translate CDDTs into an interpretable form.
- Continuous DDTs with controllers (CDDT-controllers): We modify CDDT leaf nodes to utilize linear controllers rather than static distributions.
- ICCTs with static leaf distributions (ICCT-static): We modify the leaf architecture of our ICCTs to utilize static distributions for each leaf. Comparing ICCTs and ICCTs-static displays the effectiveness of the addition of sparse linear sub-controllers.
- ICCT with complete linear sub-controllers (ICCT-complete): We allow the leaf controllers to maintain weights over all features (no sparsity enforced).
- ICCT with L1-regularized controllers (ICCT-L1-sparse): We achieve sparsity via L1-regularization applied to ICCT-complete. While this baseline produces sparse sub-controllers, there are drawbacks limiting its interpretability. L1-regularization enforces weights to be near-zero rather than exactly

zero. These small weights must be represented within decision-nodes and limit the interpretability.

- **Multi-layer Perceptron (MLP)** - We maintain three variants of an MLP. The first contains a very large number of parameters (denoted MLP-Max), typically utilized in continuous control. The second maintains approximately the same number of parameters of our ICCT at initialization (denoted MLP-Upper). The last maintains the same number of *active* parameters as our ICCT (denoted MLP-Lower).
- **Decision Tree (DT)**: We train a DT via CART [11] on state-action pairs generated from MLP-Max.

We note that the methods of CDDT and CDDT-controllers can be converted into an interpretable form post-hoc. Post-conversion, these approaches will be reported as CDDT-crisp and CDDT-controllers-crisp.

7.2 Discussion

We present the results of our trained policies in Table 1. We provide the performance of each method alongside the associated complexity of each benchmark in Table 1 across three sections, with the top section representing interpretable approaches that maintain static distributions at their leaves, the middle section containing interpretable approaches that maintain linear controllers at their leaves, and the bottom section containing black-box methods.

Static Leaf Distributions (Top): The frameworks of DT, CDDT-Crisp, ICCT-static maintain similar representations and are equal in terms of interpretability given that the approaches have the same depth. We see that across five of the six control domains, ICCT-static is able to widely outperform both the DT and CDDT-Crisp model. In complex autonomous driving domains such as Multi-Lane Ring, we are able to outperform the prior work by 91.3% and a DT by 152.7% while maintaining 9x less parameters.

Controller Leaf Distributions (Middle): Here, we rank frameworks by their relative interpretability. As the sparsity of the sub-controller decreases, the interpretability diminishes. We see that most approaches are able to achieve the maximum performance in the simple domain of Inverted Pendulum. However, CDDT-controllers-crisp encounters an inconsistency issue from the crispification procedure of [48, 41] and achieves very low performance. In regards to interpretability-performance tradeoff, in Inverted Pendulum, we see that as sparsity decreases within the sub-controller, a lower-depth ICCT can be used to achieve an equally high-performing policy. We note that across all domains, we do not find such a linear relationship. We provide additional results within

the supplementary material that provide deeper insight into the interpretability-performance tradeoff.

Black-Box Approaches (Bottom): MLP-based approaches and fuzzy DDTs are not interpretable. While the associated approaches perform well across many of the six domains, the lack of interpretability limits the utility of such frameworks in the real-world. We see that in half the domains, highly-parameterized architectures are required to learn good policies.

Comparison Across All Approaches: We see that across all continuous control domains, CDDT-Crisp and CDDT-controllers Crisp typically are the lowest-performing models. This displays the drawbacks of the crispification procedure of [48, 41] and the resultant performance inconsistency. Comparing our ICCTs to black-box models, we see that in all domains, we parity or outperform deep highly-parameterized models in performance while reducing the number of parameters required by orders of magnitude. In the difficult Multi-Lane Ring scenario, we see to we can outperform MLPs by 33% on average while achieving a 300x-600x reduction in the number of policy parameters required.

Overall, we find extremely positive support for our Interpretable Continuous Control Trees, displaying the ability to at least parity black-box approaches while maintaining high interpretability. Our novel architecture and training procedure provide a strong step towards providing solutions for two grand challenges in interpretableML: (1) Optimizing sparse logical models such as DTs and (10) Interpretable RL.

Future Work: In planned work, we propose a deepening algorithm to dynamically grow ICCTs. In the supplementary, we present a sample of our deepening algorithm, which can currently be used to alleviate the need to set the number of ICCT leaves a priori.

Limitations: Continuous control outputs (such as predicting a steering angle) may not be interpretable to end-users and may require post-processing to enhance a user’s understanding, and the relationship between controller sparsity, tree depth, and interpretability is not clear, making controller sparsity and tree depth difficult-to-define hyperparameters.

8 Conclusion

In this work, we present a novel tree-based model for continuous control, ICCTs and show ICCTs have competitive performance to that of deep neural networks across six continuous control domains while maintaining high interpretability. The maintenance of both high performance and high interpretability within our method provides an architecture that would be beneficial for real-world deployment of autonomous systems.

References

- [1] Amina Adadi and Mohammed Berrada. Peeking inside the black-box: a survey on explainable artificial intelligence (xai). *IEEE access*, 6:52138–52160, 2018.
- [2] Elaine Angelino, Nicholas Larus-Stone, Daniel Alabi, Margo Seltzer, and Cynthia Rudin. Learning certifiably optimal rule lists for categorical data. *The Journal of Machine Learning Research*, 18(1):8753–8830, 2017.
- [3] Lisa Anne Hendricks, Ronghang Hu, Trevor Darrell, and Zeynep Akata. Grounding visual explanations. In *Proceedings of the European Conference on Computer Vision (ECCV)*, pages 264–279, 2018.
- [4] Avijit Banerjee and Radhakant Padhi. Nonlinear guidance and autopilot design for lunar soft landing. In *2018 AIAA Guidance, Navigation, and Control Conference*, page 1872, 2018.
- [5] Pietro Barbiero, Gabriele Ciravegna, Dobrik Georgiev, and Francesco Giannini. Pytorch, explain! a python library for logic explained networks. 2021.
- [6] J Basak. Online adaptive decision trees. *Neural computation*, 16(9):1959–1981, 2004.
- [7] Osbert Bastani, Yewen Pu, and Armando Solar-Lezama. Verifiable reinforcement learning via policy extraction. In S. Bengio, H. Wallach, H. Larochelle, K. Grauman, N. Cesa-Bianchi, and R. Garnett, editors, *Advances in Neural Information Processing Systems*, volume 31. Curran Associates, Inc., 2018.
- [8] Osbert Bastani, Yewen Pu, and Armando Solar-Lezama. Verifiable reinforcement learning via policy extraction. In *NeurIPS*, 2018.
- [9] Yoshua Bengio, Nicholas Léonard, and Aaron C. Courville. Estimating or propagating gradients through stochastic neurons for conditional computation. *ArXiv*, abs/1308.3432, 2013.
- [10] Umang Bhatt, Alice Xiang, Shubham Sharma, Adrian Weller, Ankur Taly, Yunhan Jia, Joydeep Ghosh, Ruchir Puri, José M. F. Moura, and Peter Eckersley. Explainable machine learning in deployment, 2019.
- [11] Leo Breiman, Jerome H. Friedman, Richard A. Olshen, and C. J. Stone. Classification and regression trees. 1983.
- [12] Greg Brockman, Vicki Cheung, Ludwig Pettersson, Jonas Schneider, John Schulman, Jie Tang, and Wojciech Zaremba. Openai gym. *arXiv preprint arXiv:1606.01540*, 2016.
- [13] Chaofan Chen and Cynthia Rudin. An optimization approach to learning falling rule lists. *arXiv preprint arXiv:1710.02572*, 2017.
- [14] Gabriele Ciravegna, Pietro Barbiero, Francesco Giannini, M. Gori, Pietro Li’o, Marco Maggini, and S. Melacci. Logic explained networks. *ArXiv*, abs/2108.05149, 2021.
- [15] Jiaxun Cui, William Macke, Harel Yedidsion, Aastha Goyal, Daniel Urielli, and Peter Stone. Scalable multiagent driving policies for reducing traffic congestion. *ArXiv*, abs/2103.00058, 2021.
- [16] George V. Cybenko. Approximation by superpositions of a sigmoidal function. *Mathematics of Control, Signals and Systems*, 2:303–314, 1989.
- [17] Finale Doshi-Velez and Been Kim. Towards a rigorous science of interpretable machine learning. *arXiv preprint arXiv:1702.08608*, 2017.
- [18] Nicholas Frosst and Geoffrey E. Hinton. Distilling a neural network into a soft decision tree. *ArXiv*, abs/1711.09784, 2017.
- [19] Scott Fujimoto, Herke van Hoof, and David Meger. Addressing function approximation error in actor-critic methods. *ArXiv*, abs/1802.09477, 2018.
- [20] Abhishek Ghose and Balaraman Ravindran. Interpretability with accurate small models. *Frontiers in Artificial Intelligence*, 3, 2020.
- [21] Ian Goodfellow, Yoshua Bengio, and Aaron Courville. *Deep Learning*. MIT Press.
- [22] Tuomas Haarnoja, Aurick Zhou, Pieter Abbeel, and Sergey Levine. Soft actor-critic: Off-policy maximum entropy deep reinforcement learning with a stochastic actor. In *International conference on machine learning*, pages 1861–1870. PMLR, 2018.
- [23] Tuomas Haarnoja, Aurick Zhou, Kristian Hartikainen, George Tucker, Sehoon Ha, Jie Tan, Vikash Kumar, Henry Zhu, Abhishek Gupta, Pieter Abbeel, et al. Soft actor-critic algorithms and applications. *arXiv preprint arXiv:1812.05905*, 2018.
- [24] Daniel Hein, Steffen Limmer, and Thomas A. Runkler. Interpretable control by reinforcement learning. *ArXiv*, abs/2007.09964, 2020.

- [25] Lisa Anne Hendricks, Ronghang Hu, Trevor Darrell, and Zeynep Akata. Generating counterfactual explanations with natural language. *arXiv preprint arXiv:1806.09809*, 2018.
- [26] John M Jumper, Richard Evans, Alexander Pritzel, Tim Green, Michael Figurnov, Olaf Ronneberger, Kathryn Tunyasuvunakool, Russ Bates, Augustin Zidek, Anna Potapenko, Alex Bridgland, Clemens Meyer, Simon A A Kohl, Andy Ballard, Andrew Cowie, Bernardino Romera-Paredes, Stanislav Nikolov, Rishub Jain, Jonas Adler, Trevor Back, Stig Petersen, David A. Reiman, Ellen Clancy, Michal Zielinski, Martin Steinegger, Michalina Pacholska, Tamas Berghammer, Sebastian Bodenstein, David Silver, Oriol Vinyals, Andrew W. Senior, Koray Kavukcuoglu, Pushmeet Kohli, and Demis Hassabis. Highly accurate protein structure prediction with alphafold. *Nature*, 596:583 – 589, 2021.
- [27] Dmitry Kalashnikov, Alex Irpan, Peter Pastor, Julian Ibarz, Alexander Herzog, Eric Jang, Deirdre Quillen, Ethan Holly, Mrinal Kalakrishnan, Vincent Vanhoucke, and Sergey Levine. Qt-opt: Scalable deep reinforcement learning for vision-based robotic manipulation. *ArXiv*, abs/1806.10293, 2018.
- [28] Been Kim. Interactive and interpretable machine learning models for human machine collaboration. 2015.
- [29] Jinkyu Kim and John F. Canny. Interpretable learning for self-driving cars by visualizing causal attention. *2017 IEEE International Conference on Computer Vision (ICCV)*, pages 2961–2969, 2017.
- [30] Peter Kotschieder, Madalina Fiterau, Antonio Criminisi, and Samuel Rota Buló. Deep neural decision forests. In *Proceedings of the IEEE international conference on computer vision*, pages 1467–1475, 2015.
- [31] Himabindu Lakkaraju, Stephen H. Bach, and Jure Leskovec. Interpretable decision sets: A joint framework for description and prediction. In *Proceedings of the 22nd ACM SIGKDD International Conference on Knowledge Discovery and Data Mining*, KDD ’16, page 1675–1684, New York, NY, USA, 2016. Association for Computing Machinery.
- [32] Dmitry Laptev and Joachim M Buhmann. Convolutional decision trees for feature learning and segmentation. In *German Conference on Pattern Recognition*, pages 95–106. Springer, 2014.
- [33] Benjamin Letham, Cynthia Rudin, Tyler H McCormick, David Madigan, et al. Interpretable classifiers using rules and bayesian analysis: Building a better stroke prediction model. *The Annals of Applied Statistics*, 9(3):1350–1371, 2015.
- [34] Edouard Leurent. An environment for autonomous driving decision-making. <https://github.com/eleurent/highway-env>, 2018.
- [35] Timothy P. Lillicrap, Jonathan J. Hunt, Alexander Pritzel, Nicolas Manfred Otto Heess, Tom Erez, Yuval Tassa, David Silver, and Daan Wierstra. Continuous control with deep reinforcement learning. *CoRR*, abs/1509.02971, 2016.
- [36] Pantelis Linardatos, Vasilis Papastefanopoulos, and S. Kotsiantis. Explainable ai: A review of machine learning interpretability methods. *Entropy*, 23, 2021.
- [37] Zachary C Lipton. The mythos of model interpretability: In machine learning, the concept of interpretability is both important and slippery. *Queue*, 16(3):31–57, 2018.
- [38] Ofir Nachum, Shixiang Shane Gu, Honglak Lee, and Sergey Levine. Data-efficient hierarchical reinforcement learning. In *NeurIPS*, 2018.
- [39] Chris Olah, Arvind Satyanarayan, Ian Johnson, Shan Carter, Ludwig Schubert, Katherine Ye, and Alexander Mordvintsev. The building blocks of interpretability. *Distill*, 3(3):e10, 2018.
- [40] C Olaru and L Wehenkel. A complete fuzzy decision tree technique. *Fuzzy sets and systems*, 138(2):221–254, 2003.
- [41] Rohan R. Paleja, Andrew Silva, Letian Chen, and Matthew Gombolay. Interpretable and personalized apprenticeship scheduling: Learning interpretable scheduling policies from heterogeneous user demonstrations. 2020.
- [42] Ian Parberry. *Introduction to Game Physics with Box2D*. CRC Press, 2017.
- [43] C. Ribeiro and M. Tulio. Model-agnostic explanations and evaluation of machine learning. 2019.
- [44] C. Rudin. Stop explaining black box machine learning models for high stakes decisions and use interpretable models instead. *Nature Machine Intelligence*, 1:206–215, 2018.

- [45] Cynthia Rudin, Chaofan Chen, Zhi Chen, Haiyang Huang, Lesia Semenova, and Chudi Zhong. Interpretable machine learning: Fundamental principles and 10 grand challenges. *ArXiv*, abs/2103.11251, 2021.
- [46] John Schulman, Filip Wolski, Prafulla Dhariwal, Alec Radford, and Oleg Klimov. Proximal policy optimization algorithms. *ArXiv*, abs/1707.06347, 2017.
- [47] Rastko R. Selmic and Frank L. Lewis. Neural-network approximation of piecewise continuous functions: application to friction compensation. *IEEE transactions on neural networks*, 13 3:745–51, 2002.
- [48] Andrew Silva and M. Gombolay. Prolonets: Neural-encoding human experts’ domain knowledge to warm start reinforcement learning. *ArXiv*, abs/1902.06007, 2019.
- [49] Alberto Suárez and James F Lutsko. Globally optimal fuzzy decision trees for classification and regression. *IEEE Transactions on Pattern Analysis and Machine Intelligence*, 21(12):1297–1311, 1999.
- [50] Ryutaro Tanno, Kai Arulkumaran, Daniel C. Alexander, Antonio Criminisi, and Aditya V. Nori. Adaptive neural trees. *arXiv preprint arXiv:1807.06699*, 2018.
- [51] Emanuel Todorov, Tom Erez, and Yuval Tassa. Mujoco: A physics engine for model-based control. In *2012 IEEE/RSJ International Conference on Intelligent Robots and Systems*, pages 5026–5033. IEEE, 2012.
- [52] Paul Voigt and Axel Von dem Bussche. The eu general data protection regulation (gdpr). *A Practical Guide, 1st Ed., Cham: Springer International Publishing*, 2017.
- [53] Sholom M. Weiss and Nitin Indurkha. Rule-based machine learning methods for functional prediction. *Journal of Artificial Intelligence Research*, 3:383–403, 1995.
- [54] Cathy Wu, Aboudy Kreidieh, Kanaad Parvate, Eugene Vinitsky, and Alexandre M. Bayen. Flow: Architecture and benchmarking for reinforcement learning in traffic control. *ArXiv*, abs/1710.05465, 2017.
- [55] Mike Wu, Michael C Hughes, Sonali Parbhoo, Maurizio Zazzi, Volker Roth, and Finale Doshi-Velez. Beyond sparsity: Tree regularization of deep models for interpretability. In *Thirty-Second AAAI Conference on Artificial Intelligence*, 2018.

Supplementary: Learning Interpretable, High-Performing Policies for Continuous Control Problems

Rohan Paleja*, Yaru Niu*, Andrew Silva, Chace Ritchie, Sugju Choi, Matthew Gombolay
Atlanta, GA 30332

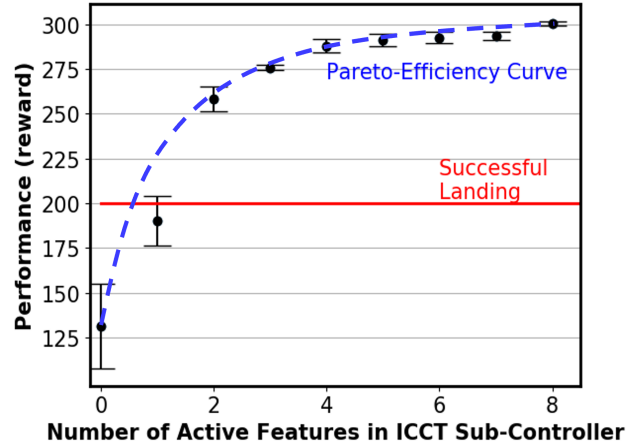
Georgia Institute of Technology

{rohan.paleja, yaruniu, andrew.silva, critchie7, schoi424, matthew.gombolay}@gatech.edu

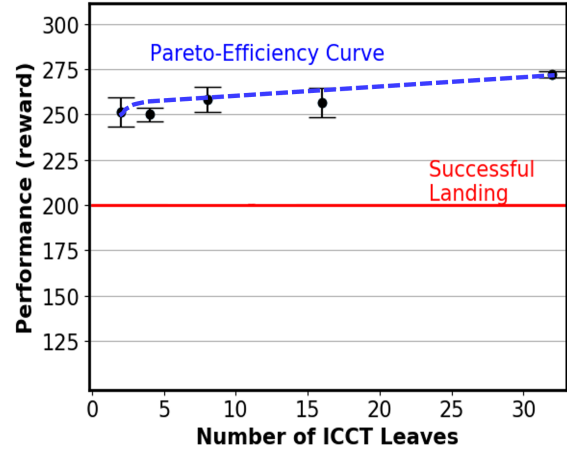
1 Interpretability Performance Tradeoff

In our paper, we briefly discuss how ICCT performance changes with respect to the number of active features within our linear sub-controllers and depth of the learned policies. [4] mentions that decision trees are interpretable because of their simplicity and that there is a cognitive limit on how complex a model can be while also being understandable. Accordingly, for our ICCTs to maximize interpretability, we emphasize the sparsity of our sub-controllers and attempt to minimize the depth of our ICCTs. Here, we present a deeper analysis by displaying the performance of our ICCTs while varying the number of active features, e , from ICCT-static to ICCT-complete (Figure 1a) and varying the number of leaves maintained within the ICCT from $l = 2$ to $l = 32$. We conduct our ablation study within Lunar Lander.

In Figure 1a, we show how the performance of our ICCTs change as a function of active features in the Sub-Controller. Here, we fix the number of ICCT leaves to 8. We see that as the number of active features increase, the performance also increases. However, there is a tradeoff in interpretability. As above 200 reward is considered successful in this domain, a domain expert may determine a point on the Pareto-Efficiency curve that maximizes the interpretability-performance tradeoff. In Figure 1b, we show how the performance of our ICCTs change as a function of tree depth, while fixing the number of active features in the ICCT sub-controller to two. We see a similar, albeit weaker, relationship between performance and interpretability. As model complexity increases, there is a slight gain in performance and with a much larger decrease in interpretability. The gentle slope of the Pareto-Efficiency curve provides insight into the interpretability-performance tradeoff for ICCT depth.



(a) ICCT Framework



(b) Example Learned Decision Tree in Lunar Lander

Figure 1: In this figure, we display the interpretability-performance tradeoff of our ICCTs with respect to active features within our linear sub-controllers (Figure 1a) and tree depth (Figure 1b). Within each figure, we display the Pareto-Efficiency Curve and denote the reward required for a successful lunar landing as defined by [1].

2 Dynamic Depth

In this section, we present a dynamic deepening algorithm here drawing inspiration from [8]. Allowing our ICCTs to automatically deepen and increase in complexity has several advantages. In continuous control, it is typical that a deployed policy may encounter a covariate shift in a real-world setting [7]. As such, our ICCT may need to change to account for features previously thought unimportant. Dynamic deepening would allow our ICCTs to mitigate the encountered covariate shift and represent additional complexities when deployed. Furthermore, the ability to deepen eliminates the need to set the tree depth a priori.

Algorithm 1 Dynamic Deepening Procedure

Input: Pretrained ICCT P , deepened ICCT P_{deep} , controller sparsity e

```

1: for  $i$  epochs do
2:   Collect trajectory rollouts,  $\tau$ , with  $P$ 
3:    $P, P_{deep} \leftarrow \text{NETWORK\_UPDATE}(P, P_{deep})$ 
4:    $\vec{H}, \vec{H}_{deep} \leftarrow \text{CALCULATE\_LEAF\_ENTROPIES}(P, P_{deep}, \tau)$ 
5:   if  $H(P_{deep}) + \epsilon < H(P)$  then
6:      $P \leftarrow P_{deep}$ 
7:      $P_{deep} \leftarrow \text{DEEPEN}(P_{deep})$ 
8:   end if
9: end for
    
```

Our proposed procedure for deepening is shown in Algorithm 1. This procedure should be conducted after a ICCT model, P , has been pretrained with an initial dataset (e.g., with simulated data for transfer to the real world). At initialization of the dynamic deepening procedure, two ICCT models are maintained, a shallow pre-trained version, P , and deeper-by-one-depth version P_{deep} . Both models utilize the same controller sparsity e . The deepened ICCT is initialized so that the top-level weights match that of P , and lower-level weights are randomly initialized. During deployment, the pre-trained ICCT model, P is utilized to collect trajectory rollouts, τ , as shown in Line 1 of Algorithm 1. Given these trajectory rollouts and associated rewards, both models are updated via gradient descent, as shown by the function `NETWORK_UPDATE` in Line 3. P is updated via Equation 2 in our main paper. As we do not have access to rollout trajectories for P_{deep} , the model update is simulated by utilizing the likelihood that P_{deep} will take similar actions to P given the states within τ . In Line 4 of Algorithm 1 (`CALCULATE_LEAF_ENTROPIES`), we calculate the entropy across each leaf within P and P_{deep} . As our leaf nodes are input-parameterized (based on state), we utilize the sample of trajectories collected in Line 2 to estimate the leaf entropy. Here, \vec{H} and \vec{H}_{deep} represent

a vector of leaf entropies. The deeper ICCT has more leaves (generated via the deepening procedure) and, thus, \vec{H}_{deep} is a higher-dimensional vector. In Line 5 of Algorithm 1, we compare the entropy of adjacent leaf nodes between P and P_{deep} . For example, in the case where we have P as a two-leaf tree and P_{deep} as a four-leaf tree, if the entropy of the left leaf node of P is at least ϵ greater than that of the combined entropy of the two left leaf nodes of P_{deep} , P_{deep} has learned a leaf distribution that is more precise in representing high-performance control behavior. Thus, in Line 6 and 7 of Algorithm 1, the shallow model, P , is updated the additional leaves of the deeper model, P_{deep} , and the deeper model, P_{deep} , is deepened by an additional level for each decision tree path that had lower entropy (determined in Line 5). This procedure continues for a set number of predefined epochs.

3 General Function for Differentiable Crispification

In this section, we provide a function to generalize the procedure of our decision node crispification and decision outcome crispification.

Algorithm 2 Differentiable Argument Max Function for Crispification

Input: Logits \vec{q}

Output: One-Hot Vector \vec{h}

```

1:  $\vec{h}_{soft} \leftarrow f(\vec{q})$ 
2:  $\vec{h}_{hard} \leftarrow g(f(\vec{q}))$ 
3:  $\vec{h} = \vec{h}_{hard} + \vec{h}_{soft} - \text{STOP\_GRAD}(\vec{h}_{soft})$ 
    
```

Similar to [2], we present a function call (in Algorithm 2) that can be utilized to maintain gradients over a non-differentiable one-hot operation. The function takes in a set of logits, \vec{q} and applies a softmax operation, denoted by f , to output \vec{h}_{soft} , as shown in Line 1. In Line 2, the logits are transformed using a softmax followed by a one-hot procedure, g , causing the removal of gradient information, producing \vec{h}_{hard} . In line 3, we combine \vec{h}_{soft} , \vec{h}_{hard} , and $\text{STOP_GRAD}(\vec{h}_{soft})$ to output \vec{h} . The outputted value of \vec{h} is equal to that of \vec{h}_{hard} . However, the gradient maintained within \vec{h} is that associated with \vec{h}_{soft} . Automatic differentiation frameworks can then utilize the outputted term to perform backpropagation.

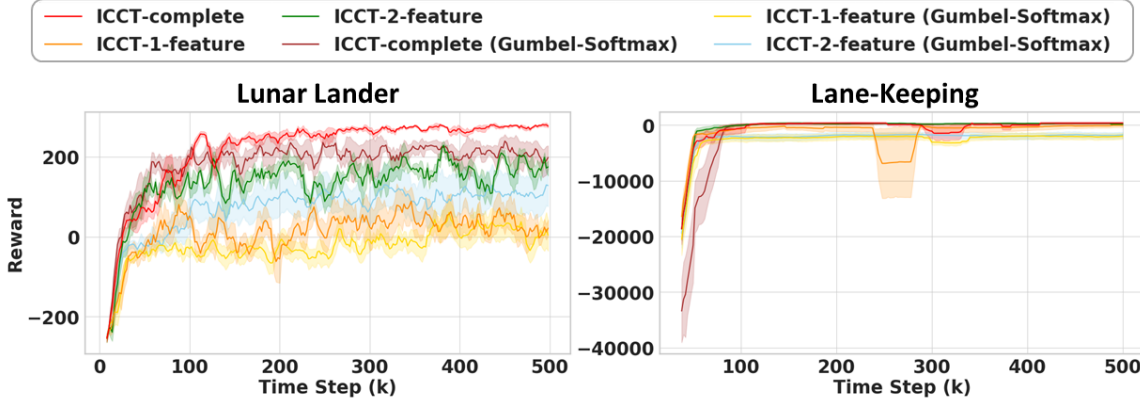


Figure 2: This figure displays the average running rollout rewards of six methods for the ablation study during training. The results are averaged over 5 seeds, and the shadow region represents the standard error.

Table 1: Performance Comparison between ICCTs utilizing the differentiable crispification (and enforcing sparsity) procedure discussed in Section 4 within the main paper, ICCTs utilizing a Gumbel-Softmax differentiable crispification (and enforcing sparsity) procedure, and crisp ICCTs utilizing a Gumbel-Softmax differentiable crispification (and enforcing sparsity) procedure. We present findings across Lunar Lander and Lane-Keeping

Method	Lunar Lander	Lane-Keeping
ICCT-complete	300.5 ± 1.2	476.6 ± 3.1
ICCT-complete (Gumbel-Softmax)	276.7 ± 7.0	412.6 ± 31.3
ICCT-complete (Gumbel-Softmax, Crisp)	239.0 ± 18.9	309.1 ± 94.6
ICCT-1-feature	190.1 ± 13.7	437.6 ± 7.0
ICCT-1-feature (Gumbel-Softmax)	113.2 ± 43.1	-853.4 ± 333.2
ICCT-1-feature (Gumbel-Softmax, Crisp)	-20.1 ± 50.0	-658.114 ± 345.3
ICCT-2-feature	258.4 ± 7.0	458.5 ± 6.3
ICCT-2-feature (Gumbel-Softmax)	161.7 ± 54.8	-560.6 ± 251.6
ICCT-2-feature (Gumbel-Softmax, Crisp)	62.3 ± 82.2	-945.0 ± 331.0

4 Differentiable Crispification and Enforcing Sparsity with Gumbel-Softmax

In this section, we provide an ablation study where we utilize a Gumbel-Softmax [3] function to perform decision node crispification, perform decision outcome crispification, and enforce sub-controller sparsity. The difference of using a Gumbel-Softmax function in ICCT is turning the softmax function f introduced in Section 4 within the main paper to f' as follows:

$$f'(\vec{w}_i)_k = \frac{\exp\left(\frac{w_i^k + g_i^k}{\tau}\right)}{\sum_j \exp\left(\frac{w_i^j + g_i^j}{\tau}\right)} \quad (1)$$

where \vec{w}_i is a vector composed of m elements $w_i^1, w_i^2, \dots, w_i^m$, and $g_i^1, g_i^2, \dots, g_i^m$ are i.i.d samples from Gumbel(0, 1) distribution [3]. Here, we compare the performance of ICCT-complete, ICCT-1-feature, and ICCT-2-feature to their variants using Gumbel-Softmax in Lunar Lander and Lane-Keeping. All the

methods and their corresponding variants are trained using the same hyperparameters.

From the results shown in Figure 2 and Table 1, we find that the addition of Gumbel noise reduces performance by a wide margin. Furthermore, comparing crisp ICCTs utilizing Gumbel-Softmax to ICCTs utilizing Gumbel-Softmax, we see that due to the sampling procedure within the Gumbel-Softmax, an inconsistency issue arises between non-crisp and crisp performance.

5 Learning Curves

In Figure 3, we display the learning curves of the eleven methods across six domains shown in Table 1 of the main paper. In general, ICCT-complete has competitive or better performance with regards to running average rollout rewards and convergence rate, compared to MLP-Max, MLP-Upper and fuzzy DDTs in Inverted Pendulum, Lunar Lander, Lane-Keeping, Sing-Lane Ring, and Multi-Lane Ring, while maintaining

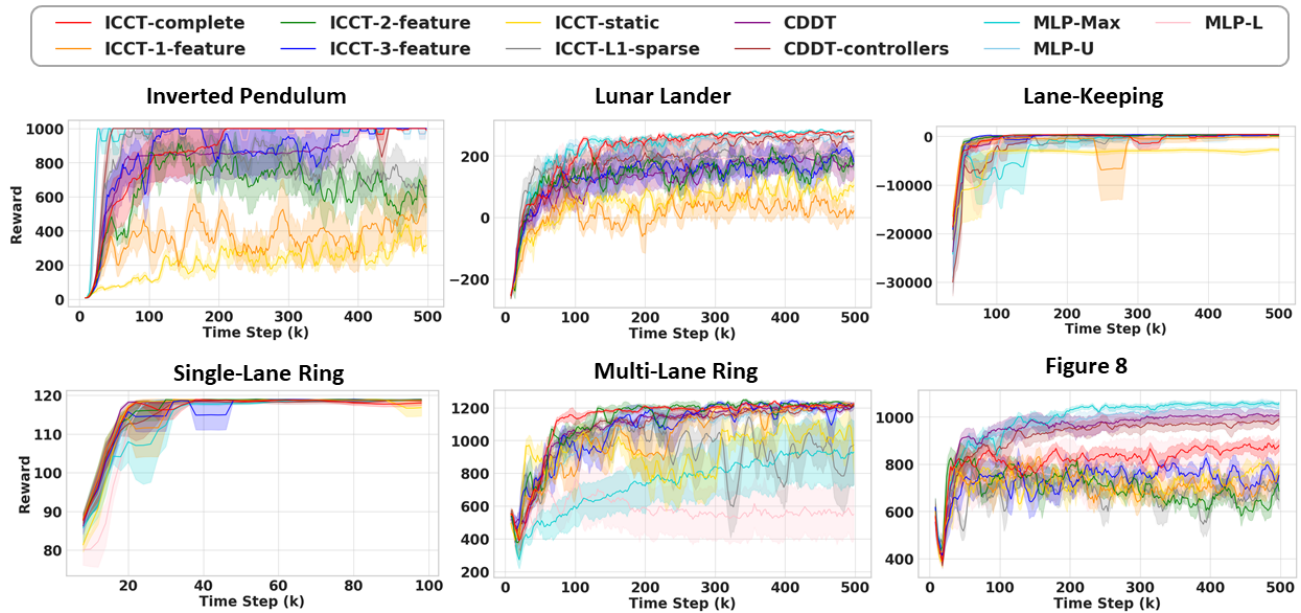


Figure 3: In this figure, we display the learning curves of eleven methods in six domains shown in the main paper. The rewards are rollout rewards throughout the training process. The curves in 5 domains except Lane-Keeping are smoothed by a sliding window of size 5, the curves in Lane-Keeping are smoothed by a sliding window of size 20. The shadow region depicts the standard error across 5 seeds.

interpretability. As the sparsity of the linear sub-controller increases, the performance of ICCT gradually drops down, while ICCT-3-feature and ICCT-2-feature still have comparable or better performance compared to MLP-Lower and ICCT-L1-sparse, while maintaining high interpretability.

6 Environments

We provide detailed descriptions for three common continuous control problems and including Inverted Pendulum, Lunar-Lander, and Lane-Keeping, and three environments from the popular autonomous driving simulator, Flow [10], including Single-Lane Ring, Multi-Lane Ring, and Figure 8.

Inverted Pendulum: Inverted Pendulum (Figure 4(a)) is provided by MuJoCo [9] and OpenAI Gym [1]. The observation includes the cart position, velocity, pole angle, and pole angular velocity. The goal is to apply a force to the cart to balance a pole on it and prevent the pole from falling. A plus one reward is provided at each timestep provided if the pole keeps upright at each time step.

Lunar Lander: Lunar Lander (Figure 4(b)) is a game provided by Box2D [6] and OpenAI Gym. The goal is to land a lunar lander as close to a landing pad between the flags. The observation is 8-dimensional including the lander’s current position, linear velocity,

tilt, angular velocity, and information about ground contact. The continuous action space is two dimensional for controlling the main engine thruster and side thrusters. At each timestep, the lander reward is determined by a proximity to the landing pad, whether each leg is touching the landing pad, and a fuel cost. The episode ends if the lander crashes and a terminal reward of -100 is provided. If the lander is successful at landing, a positive terminal reward of 100 is provided.

Lane-Keeping: Lane-Keeping (Figure 4(c)) is a domain with continuous actions within highway-env [5]. The observation is 12-dimensional, which consists of the vehicle’s lateral position, heading, lateral speed, yaw rate, linear, lateral, and angular velocity, and the lane information. The action is the steering angle to control the vehicle. At each time step, +1 reward will be provided if the vehicle can keep in the center of the lane. The reward decreases as the vehicle drives away from the lane center. The terminal condition within this domain is a maximum timestep of 500.

Flow Domains [10]: Each of the following domains are custom continuous actions domains provided within the Flow deep reinforcement learning framework for mixed autonomy traffic scenarios. Flow utilizes the SUMO traffic simulator, which allows for both autonomous agents and simulated human agents. The simulated human agents are constructed by adjusting the noise factor present within their acceleration and deceleration control. Stabilization of traffic is de-

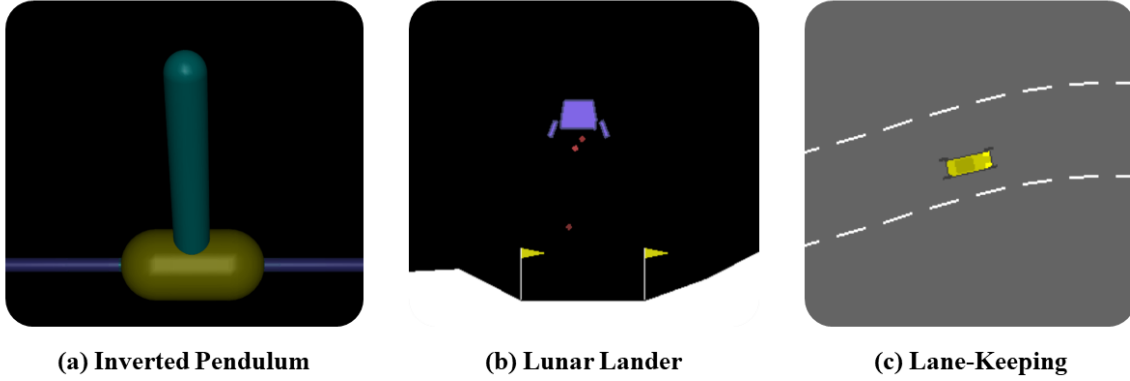


Figure 4: This figure displays the three non-traffic environments we utilized including Inverted Pendulum, Lunar Lander, and Lane-Keeping.

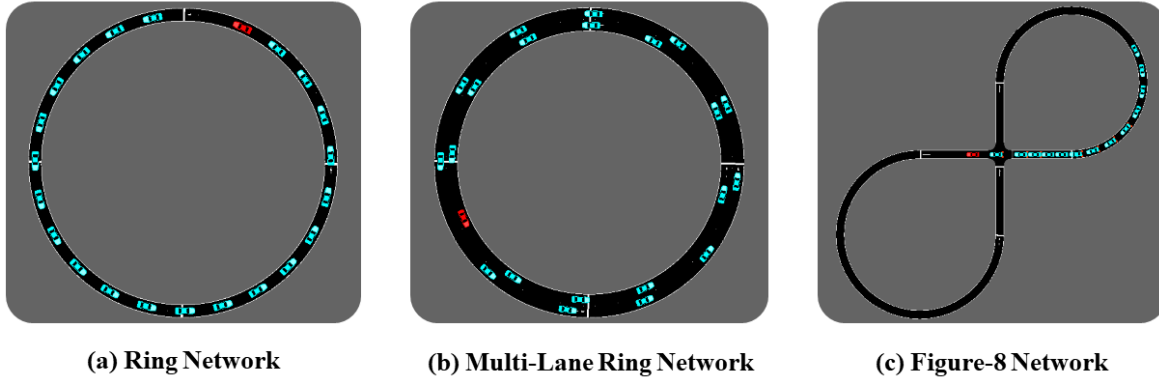


Figure 5: In this figure, we display the configuration of each Flow network used in our experimentation. In each image, the red vehicle is the autonomous agent that utilizes the learned control policy to stabilize traffic flow. Each cyan vehicle is a simulated human vehicle which contains a noisy acceleration behavior, the severity of which is defined by the user.

defined as the average velocity of all vehicles approaching a set value for velocity. The general observation includes the global positions and velocity of all vehicles in the network. These are normalized based upon the length and max velocity for the network, which is defined by the user, and then combined into a single 1-Dimensional array with a length that is double the number of vehicles present. The reward is measured by how closely the network’s average velocity matches the user-defined average velocity. The episode is terminated if any collision between two vehicles is detected, or preset time steps are executed.

Flow Single-Lane Ring Network: The Single-Lane Ring Network (Figure 5(a)) is a ring road network, with the objective being to stabilize the flow of all traffic within the network. A control policy must apply acceleration commands to an autonomous agent in order to stabilize the flow. There are 21 human vehicles and 1 ego vehicle, with a maximum time step of 750.

Flow Multi-Lane Ring Network: The Multi-Lane Ring network (Figure 5(b)) is a complex ring road network consisting of multiple lanes of traffic, with the objective being to stabilize the flow of all traffic within the network. The observation for this network includes the general observation for Flow networks, as well as the current lane index for each vehicle. The network holds 21 human vehicle and 1 ego vehicle. A control policy must apply acceleration commands and lane changing commands (a continuous value from -1 to 1) to the ego vehicle in order to stabilize the flow of traffic between both lanes. The maximum step in this domain is set to 1500.

Flow Figure-8 Network: The Figure-8 Network (Figure 5(c)) is a complex Flow domain as it contains a road section where the vehicles will cross-over, which is in the center of the figure-8. The control policy must consider this congestion point when controlling the ego vehicle, applying acceleration commands to the autonomous agent in order to stabilize the flow.

The network holds 13 human vehicles besides the ego vehicle. Here the maximum time step is 1500.

7 Hyperparameters

All methods are trained using SAC with the same structure of critic network, which consists of an MLP with 2 hidden layers of 256 units. The buffer size is always set to 1000000, and the discount factor γ is always set to 0.99. In Sing-Lane Ring network, the training steps are 100000, otherwise the training steps are 500000 for all the methods. The soft update coefficient τ is set to 0.005 for ICCT-static in Inverted Pendulum, otherwise it is kept as 0.01. Then we display the learning rates (LR), batch sizes (BS) and network sizes (NS) used for the methods discussed in the paper in each domain from Table 2 to Table 7.

Table 2: Hyperparameters in Inverted Pendulum

Hyperparameter	Learning Rate	Batch Size	Network Size
ICCT-complete	3e-4	1024	2 leaves
ICCT-1-feature	6e-4	1024	8 leaves
ICCT-2-feature	5e-4	1024	4 leaves
ICCT-3-feature	5e-4	1024	2 leaves
ICCT-static	5e-4	1024	32 leaves
ICCT-L1-sparse	3e-4	256	4 leaves
CDDT	3e-4	1024	2 leaves
CDDT-controllers	3e-4	1024	2 leaves
MLP-Max	3e-4	1024	[256, 256]
MLP-U	3e-4	1024	[8, 8]
MLP-L	3e-4	1024	[6, 6]

Table 3: Hyperparameters in Lunar Lander

Hyperparameter	Actor LR	Critic LR	BS	Network Size
ICCT-complete	5e-4	5e-4	256	8 leaves
ICCT-1-feature	5e-4	5e-4	256	8 leaves
ICCT-2-feature	5e-4	5e-4	256	8 leaves
ICCT-3-feature	5e-4	5e-4	256	8 leaves
ICCT-static	5e-4	3e-4	256	32 leaves
ICCT-L1-sparse	5e-4	5e-4	256	8 leaves
CDDT	5e-4	3e-4	256	8 leaves
CDDT-controllers	5e-4	3e-4	256	8 leaves
MLP-Max	3e-4	3e-4	256	[256, 256]
MLP-U	3e-4	3e-4	256	[10, 10]
MLP-L	3e-4	3e-4	256	[6, 6]

Table 4: Hyperparameters in Lane-Keeping

Hyperparameter	Learning Rate	Batch Size	Network Size
ICCT-complete	3e-4	1024	16 leaves
ICCT-1-feature	3e-4	1024	16 leaves
ICCT-2-feature	3e-4	1024	16 leaves
ICCT-3-feature	3e-4	1024	16 leaves
ICCT-static	2e-4	1024	16 leaves
ICCT-L1-sparse	3e-4	1024	16 leaves
CDDT	3e-4	256	16 leaves
CDDT-controllers	3e-4	512	16 leaves
MLP-Max	3e-4	256	[256, 256]
MLP-U	3e-4	256	[14, 14]
MLP-L	3e-4	256	[6, 6]

Table 5: Hyperparameters in Sing-Lane Ring Network

Hyperparameter	Learning Rate	Batch Size	Network Size
ICCT-complete	5e-4	1024	16 leaves
ICCT-1-feature	5e-4	1024	16 leaves
ICCT-2-feature	5e-4	1024	16 leaves
ICCT-3-feature	5e-4	1024	16 leaves
ICCT-static	5e-4	1024	16 leaves
ICCT-L1-sparse	5e-4	1024	16 leaves
CDDT	5e-4	1024	16 leaves
CDDT-controllers	5e-4	1024	16 leaves
MLP-Max	3e-4	1024	[256, 256]
MLP-U	3e-4	1024	[12, 12]
MLP-L	3e-4	1024	[3, 3]

Table 6: Hyperparameters in Multi-Lane Ring Network

Hyperparameter	Learning Rate	Batch Size	Network Size
ICCT-complete	5e-4	1024	16 leaves
ICCT-1-feature	5e-4	1024	16 leaves
ICCT-2-feature	6e-4	1024	16 leaves
ICCT-3-feature	5e-4	1024	16 leaves
ICCT-static	5e-4	1024	16 leaves
ICCT-L1-sparse	5e-4	1024	16 leaves
CDDT	5e-4	1024	16 leaves
CDDT-controllers	5e-4	1024	16 leaves
MLP-Max	5e-4	1024	[256, 256]
MLP-U	5e-4	1024	[32, 32]
MLP-L	5e-4	1024	[3, 3]

Table 7: Hyperparameters in Figure-8 Network

Hyperparameter	Learning Rate	Batch Size	Network Size
ICCT-complete	5.5e-4	1024	16 leaves
ICCT-1-feature	6e-4	1024	16 leaves
ICCT-2-feature	6e-4	1024	16 leaves
ICCT-3-feature	7e-4	1024	16 leaves
ICCT-static	5e-4	1024	16 leaves
ICCT-L1-sparse	5e-4	1024	16 leaves
CDDT	5e-4	1024	16 leaves
CDDT-controllers	5e-4	1024	16 leaves
MLP-Max	5e-4	1024	[256, 256]
MLP-U	5e-4	1024	[20, 20]
MLP-L	5e-4	1024	[3, 3]

References

- [1] Greg Brockman, Vicki Cheung, Ludwig Pettersson, Jonas Schneider, John Schulman, Jie Tang, and Wojciech Zaremba. Openai gym. *arXiv preprint arXiv:1606.01540*, 2016.
- [2] Danijar Hafner, Timothy P. Lillicrap, Mohammad Norouzi, and Jimmy Ba. Mastering atari with discrete world models. *ArXiv*, abs/2010.02193, 2021.
- [3] Eric Jang, Shixiang Shane Gu, and Ben Poole. Categorical reparameterization with gumbel-softmax. *ArXiv*, abs/1611.01144, 2017.
- [4] Himabindu Lakkaraju, Stephen H. Bach, and Jure Leskovec. Interpretable decision sets: A joint framework for description and prediction. In *Proceedings of the 22nd ACM SIGKDD International Conference on Knowledge Discovery and Data Mining*, KDD ’16, page 1675–1684, New York, NY, USA, 2016. Association for Computing Machinery.

- [5] Edouard Leurent. An environment for autonomous driving decision-making. <https://github.com/eleurent/highway-env>, 2018.
- [6] Ian Parberry. *Introduction to Game Physics with Box2D*. CRC Press, 2017.
- [7] Xue Bin Peng, Marcin Andrychowicz, Wojciech Zaremba, and P. Abbeel. Sim-to-real transfer of robotic control with dynamics randomization. *2018 IEEE International Conference on Robotics and Automation (ICRA)*, pages 1–8, 2018.
- [8] Andrew Silva and Matthew Craig Gombolay. Encoding human domain knowledge to warm start reinforcement learning. In *AAAI*, 2021.
- [9] Emanuel Todorov, Tom Erez, and Yuval Tassa. Mujoco: A physics engine for model-based control. In *2012 IEEE/RSJ International Conference on Intelligent Robots and Systems*, pages 5026–5033. IEEE, 2012.
- [10] Cathy Wu, Aboudy Kreidieh, Kanaad Parvate, Eugene Vinitsky, and Alexandre M. Bayen. Flow: Architecture and benchmarking for reinforcement learning in traffic control. *ArXiv*, abs/1710.05465, 2017.